University Technology Petronas

Electrical & Electronics Engineering

FYPII EBB4034

Final Report

Topic: Design and Simulation of a Low Frequency Electrostatic Comb-drive Energy Harvester Using 0.35µm CMOS Technology

Mohamed Abdalla Osman

12929

Supervisor:

Dr.John Ojur Dennis

CERTIFICATION OF APPROVAL

Design and Simulation of a Low Frequency Electrostatic Comb-drive Energy Harvester with 0.35 μm CMOS Technology

by

Mohamed Abdalla Osman Mohamed

A project dissertation submitted to the
Department of Electrical & Electronic Engineering
Universiti Teknologi PETRONAS
in partial fulfilment of the requirement for the
Bachelor of Engineering (Hons)
(Electrical & Electronic Engineering)

Approved:

_____

Dr.John Ojour Dennis
Project Supervisor

UNIVERSITI TEKNOLOGI PETRONAS

TRONOH, PERAK

May 2012

CERTIFICATION OF ORIGINALITY

This is to certify that I am responsible for the work submitted in this project, that the original work is my own except as specified in the references and acknowledgements, and that the original work contained herein have not been undertaken or done by unspecified sources or persons.

_____

MOHAMED ABDALLA OSMAN

Acknowledgement

First and foremost, I thank Allah, the Most Merciful and the most Beneficent, for endowing me with health, patience, and knowledge to complete my final year project. And I also thank his almighty for being my strength and guide in the writing of this report. Without him, I would not have had the wisdom or the physical ability to do so.

My grateful thanks also go to my supervisor Dr. John Ojur Dennis for giving me the chance to proceed my project under his supervision. I also express my gratitude Mr. Abdul Aziz Yousif and Mr. Almur Abdulkareem for the great help they offered to me throughout the project progress.

Abstract

This project is to design, model and simulate an electrostatic comb-drive energy harvester. The device harvests the vibration energy from outside source and converts it into electric energy to supply wireless node sensors. Simulation is conducted using the CoventorWare software to simulate and optimize the device. CoventorWare simulation result has obtained a resonant frequency of 5 KHz.

Table of Contents

Acknowledgement I

Abstract II

Table of Contents II

List of Figures IV

List of Tables V

Introduction 1

1.1 Background of Study 1

1.2 Problem Statement 2

1.3 Objectives 2

1.4 Scope of Study 2

Literature Review 3

1.5 Electrostatic (Capacitive) Power Conversion 3

1.6 Sources of Vibrations 4

1.7 In-Plane Overlap Converter 5

1.8 Principle of Operation 7

1.9 General Model for Vibration Conversion 10

Device Modeling 13

1.10 Comb-drive Energy Harvester Structure 13

1.11 Evaluation of the Capacitance per Unit Length 15

1.11.1 Evaluation of the Maximum and Minimum Capacitances (C_{max} and C_{min}): 18

1.12 Spring Constant: 20

1.12.1 Folded-beam suspension design: 20

1.12.2 Spring Constant of Folded-beam Structure: 20

Methodology 24

1.13 Project Flow Chart 24

1.14 Gantt Chart FYP1 26

1.15 Gantt Chart FYP2 27

Results and Discussion 28

1.16 Evaluation of Equation of Motion 28
1.17 Evaluation of Spring Constant 31
1.18 Evaluation of Natural Frequency (ω_n) 32
1.19 Evaluation of Output Power 34
1.19.1 Mechanical Damping 34
1.19.2 Electrical Damping 34
1.19.3 Total Damping 35
1.19.4 Displacement 35
1.19.5 Maximum Capacitance 36
1.19.6 Energy per Cycle 36
1.19.7 Simulation Results 37
Conclusion 41
References 42
Appendices 44
1.20 Appendix I 44
1.21 Appendix II 45

List of Figures

FIGURE 1: IN-PLANE OVERLAP STRUCTURE, THE DARK AREAS REPRESENT THE FIXED ELEMENTS AND THE LIGHT AREAS, THE MOVABLE ELEMENTS COMB-DRIVE STRUCTURE PLAN VIEW. CHENGKUO LEEA ET AL [4]. 5
FIGURE 2: IN-PLANE OVERLAP CONVERTER. CHENGKUO LEE ET AL [4] 5
FIGURE 3: IN-PLANE OVERLAP CONVERTER S.ROUNDY [2] 7
FIGURE 4: ENERGY CONVERSION CYCLES. AHMED NOUNOU. HANI F. RAGAIE [4] 7
FIGURE 5: THE CHARGE-CONSTRAINED ENERGY CONVERSION CYCLE. CHENGKUO LEEA ET AL [4] 8
FIGURE 6: THE SCHEMATIC CIRCUIT OF A CAPACITIVE CONVERTER GEENG-JEN SHEU ET AL [9]. 10
FIGURE 7: SCHEMATIC OF GENERIC VIBRATION CONVERTER. S. ROUNDY ET AL [2] 11
FIGURE 8: TOP VIEW OF ENERGY HARVESTER 13
FIGURE 9: THE COMB-DRIVE ENERGY HARVESTER 13
FIGURE 10: SKETCH OF TYPICAL TWO PLATES CAPACITOR 15
FIGURE 11 : CAPACITANCE-PER-UNIT-LENGTH ($\frac{\partial C}{\partial x}$) VS COMB-DRIVE GAP (G) 17
FIGURE 12 : IN-PLANE-OVERLAP CONVERTER IN CMIN POSITION ($\Delta x = 0$) 18
FIGURE 13 : IN-PLANE-OVERLAP CONVERTER IN CMIN POSITION ($\Delta x = l$) 19
FIGURE 14: TWO FOLDED-BEAM STRUCTURE 20
FIGURE 15: MODE SHAPE OF A FOLDED BEAM WHEN FORCE F_x IS APPLIED AND STRUCTURE IS DISPLACED BY X0. TANG [10] 21
FIGURE 16:MODE SHAPE OF BEAM [AB]. TANG [10] 21
FIGURE 17 : PROJECT FLOW CHART 25
FIGURE 18: SCHEMATIC OF GENERIC VIBRATION CONVERTER. S. ROUNDY ET AL [2] 28
FIGURE 19: VARIATION OF PHASE ANGLE VS FREQUENCY RATIO R 30
FIGURE 20 : VARIATION OF AMPLITUDE VS FREQUENCY RATIO R 30
FIGURE 21 : FREQUENCY VS VIBRATING MASS 32
FIGURE 22: SCHEMATIC CROSS SECTION OF THE DEVICE 37
FIGURE 23: 3-D LAYOUT OF ENERGY HARVESTER 38
FIGURE 24: ETCH FROM BACK SIDE 38
FIGURE 25: 3-D MESHED MODEL 39
FIGURE 26: 2-D FEM SIMULATION RESULT 39
FIGURE 27: 3-D FEM SIMULATION RESULT 40

List of Tables

TABLE 1: ACCELERATION (M/S2), MAGNITUDE AND FREQUENCY OF FUNDAMENTAL VIBRATION MODE FOR VARIOUS SOURCES. S. ROUNDY ET AL [2] 4
TABLE 2: THE ENERGY HARVESTER DESIGN PARAMETERS 14
TABLE 3: GANTT CHART 26
TABLE 4: VALUES TO CALCULATE SPRING CONSTANT 31
TABLE 5: VALUES FOR NATURAL FREQUENCY CALCULATION 32
TABLE 6: : TABLE FOR MECHANICAL DAMPING CALCULATION 34
TABLE 7: : TABLE FOR ELECTRICAL DAMPING CALCULATION 34
TABLE 8 : : TABLE FOR DISPLACEMENT CALCULATION 35
TABLE 9: : TABLE FOR MAXIMUM CAPACITANCE CALCULATION 36

Introduction

1.1 Background of Study

Energy harvesting systems have emerged as a prominent research area and continue to grow rapidly. A wide range of applications are targeted for the harvesters including distributed wireless sensor nodes, recharging the batteries of large systems and running security systems in household conditions. Recent development includes the components and devices at a micro-macro scales covering materials, electronics and integration.

Energy harvesting systems have various sources from which energy can be harvested. For instance, piezoelectric materials are one of the common phenomenon utilized in energy scavenging techniques where a source provides required vibration then piezoelectric materials convert the mechanical movement (vibration) into electric current to power up electronic devices. However, electromagnetic transducers represent another technique to harvest kinetic energy (vibration). Thermoelectric energy as well is common technique to harvest energy from a heat source. A good example of thermoelectric energy harvesting is the thermoelectric wrist-watch that converts body heat into electrical power that drives the watch.

However, in this project electrostatic energy harvesting technique is used to harvest kinetic energy from a convenient vibration source into electrical energy to power up sensor nodes.

1.2 Problem Statement

Providing power supply for wireless sensors has been a focus of study in the research community on small wireless electronic devices for the past few years. Currently, batteries are the main source of power in use for wireless sensors. However, batteries does not offer the ideal solution as it has a finite limit of power and runs short of electricity over time.

An electrostatic comb-drive energy harvester would present an optimal solution with an infinite supply of power for wireless sensor nodes. The energy harvester will utilize low-level vibrations occurring in environment as a conventional power source. The MEMS-based device would then be fabricated by standard CMOS process.

1.3 Objectives

- To design and model a MEMS-based electrostatic comb-drive energy harvester.
- To simulate and optimize the device characteristics and functionality.

1.4 Scope of Study

The project investigates the design of a MEMS-based energy harvester to convert mechanical energy to electrical energy in order to provide wireless nodes with power.

Literature Review

1.5 Electrostatic (Capacitive) Power Conversion

Electrostatic generation consists of a pair of electrodes separated by a dielectric material which moves in relative to each other. This movement of electrodes changes the amount of energy stored in the capacitor which establish the mechanical to electrical conversion principle.

In order to understand the mechanical to electrical conversion a simple rectangular parallel plate capacitor would be used. The voltage across the capacitor is given by:

$$V = \frac{Qd}{\varepsilon_0 lw} \tag{1.1}$$

Where Q is charge on capacitor, d is gap between plates, l is length of the plate, w is the width of the plate, and ε_0 is the dielectric constant of free space.

Note capacitor is given by $C = \frac{\varepsilon_0 lw}{d} = \frac{Q}{V}$, if the charge is held constant then voltage value can be increased by reducing capacitance (decreasing l or w, increasing d) which is called charge-constrained method. On the other hand, if the voltage is held constant, charge can be increased by (increasing l or w, reducing d) which is called voltage-constrained method. In both cases energy stored on capacitor, which is given by (1.2), increases.

$$E = \frac{QV}{2} = \frac{CV^2}{2} = \frac{Q^2}{2V} \tag{1.2}$$

Charge-constrained conversion is much popular over voltage constrained conversation method as it requires one external charge reservoir instead of two according to S. Roundy et al [2].

Electrostatic converters have the disadvantage as existence of separate voltage source is necessary to charge up an initial voltage for conversion process. Another disadvantage is that mechanical stops must exist to prevent electrodes contact. This results in increase at amount of

mechanical damping. An excellent discussion of charge-constrained versus voltage-constrained is given by Chengkuo Lee et al [4].

1.6 Sources of Vibrations

Vibration sources provides kinetic energy necessary for the power conversion process to electrical energy, hence, details of vibration source has to be comprehensively studied to determine how much power can be converted. S. Roundy et al [2]. has discussed about common available occurring vibration sources. The study emphasizes on low-level vibrations. Table 1 lists examples of vibration sources presented in terms of frequency and acceleration magnitude of fundamental vibration mode.

Table 1: acceleration (m/s2), magnitude and frequency of fundamental vibration mode for various sources. S. Roundy et al [2]

Vibration source	**A (m/s^2)**	f_{peak}
Car engine compartment	12	200
Base of 3-axis machine tool	10	70
Blender Casing	6.4	121
Clothes dryer	3.5	121
Person nervously tapping their heel	3	1
Car Instrument panel	3	13
Door frame jus after door closes	3	125
Small microwave oven	2.5	121
HVAC vents in office building	0.2 – 1.5	60
Windows next to a busy road	0.7	100
CD on notebook computer	0.6	75
Second story floor of busy office	0.2	100

Significance of vibration sources arises in the design of vibration converters due to few reasons. First, devices have to be designed to resonate at fundamental vibration frequency. Second, the design should target low frequency vibration modes in order to achieve higher output power (output power is proportional to a^2/ω where ω is frequency of fundamental vibration mode). Third, to estimate amount of power generation, the magnitude and frequency of driving vibration must firstly be determined.

1.7 In-Plane Overlap Converter

Ahmed Nounou and Hani F. Ragaie [3] discusses the feasibility of power generation using a laterally driven comb structure based on MEMS technology. Their design utilized the in-plane overlap structure.

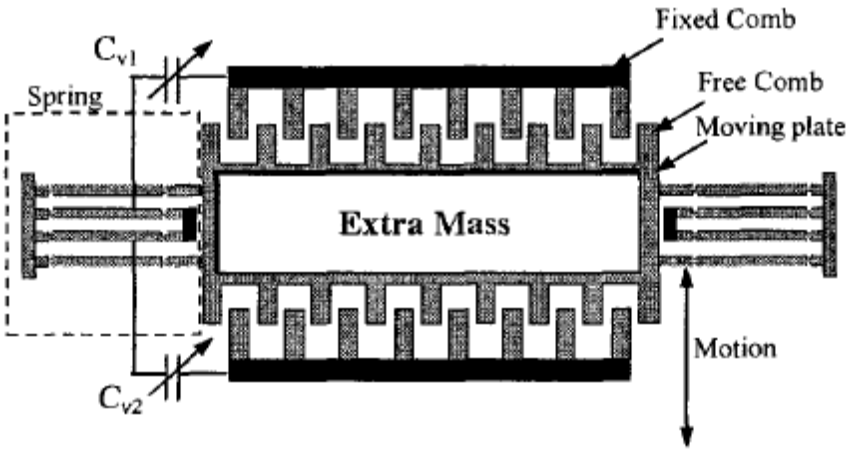

Figure 1: In-Plane Overlap Structure, the dark areas represent the fixed elements and the light areas, the movable elements Comb-Drive Structure Plan view. Chengkuo Leea et al [4].

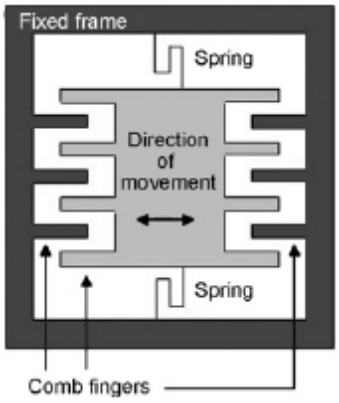

Figure 2: In-Plane Overlap Converter. Chengkuo Lee et al [4]

The in-plane overlap structure consists of a vibrating plate attached to spring that allows motion on the shown direction only. The dark areas are fixed to the substrate, while the light areas are

released structure that is free to move. The device is referred to as in-plane overlap structure because the change in capacitor value is when overlap area of the facing fingers is changing.

As shown Figure (3) an extra mass is added on top of the vibrating plate in order to acquire resonance such the low frequency as

$$f = \frac{1}{2\pi}\sqrt{\frac{k}{m}} \tag{2.1}$$

Where f is the resonant frequency, k is the spring constant, m is total mass of free structure.

Due to the symmetry of the structure, two variable capacitors exist in opposite to each other. Hence, energy conversion process takes place in two phases during steady-state operation of the converter.

1.8 Principle of Operation

The basics of electrostatic energy conversion depend essentially upon capacitance change. As for this project, the in-plane overlap electrostatic converter is used. The capacitance change takes place as overlap area between fingers vary due to vibration motion indicated by Fig(3).

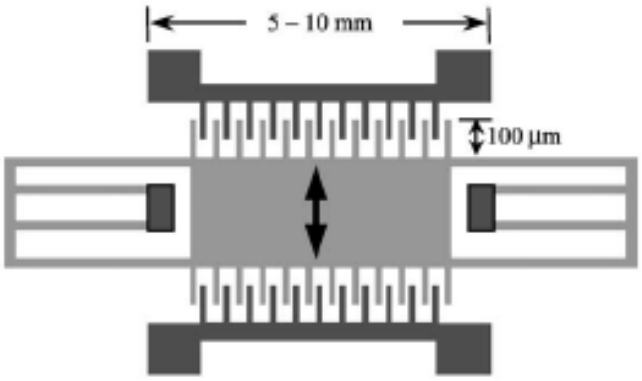

Figure 3: In-plane overlap converter S.Roundy [2]

Meninger et al [1] gives a good explanation of the advantages of charge constrained conversion against voltage constrained conversion. This project will work with charge constrained converter because two separate voltage sources are needed for voltage constrained conversion. Moreover, Chengkuo Lee et al [4] states that the charge constrained method is more popular over the voltage-constrained method as it requires just one external charge reservoir instead of two.

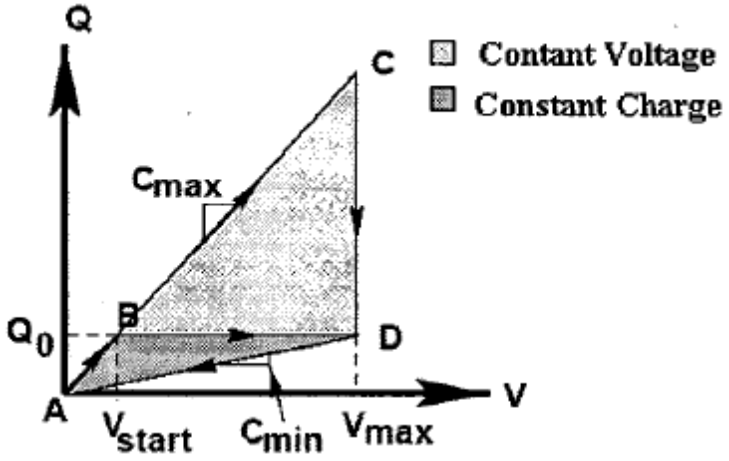

Figure 4: Energy conversion cycles. Ahmed Nounou. Hani F. Ragaie [4]

Figure (4) shows conversion cycle for both charge-constrained and voltage charge-constrained methods. It is obvious from the figure that constant voltage provides more energy but still it has many imperfections which prevent its practical existence Ahmed Nounou et al [3]. Therefore, constant charge method would be used in the design as it is the suitable implementation.

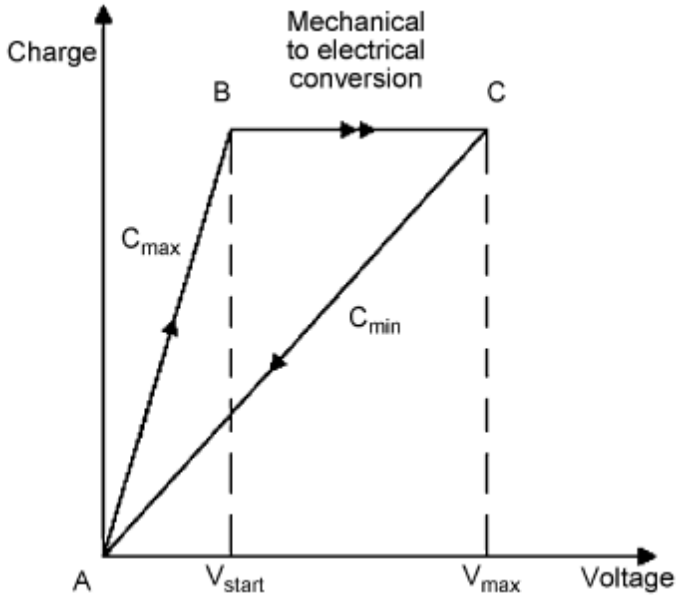

Figure 5: The charge-constrained energy conversion cycle. Chengkuo Leea et al [4]

According to Chengkuo Leea et al [4] when the structure is vibrating, the energy conversion cycle starts when the capacitance of the structure momentarily reaches an effective maximum value of C_{max}. This charging process is represented by the path from point A to point B in Fig (5). At the point B, an external charge reservoir deposits a charge across the electrodes. As a result, an effective potential difference of V_{start} can be measured across the electrodes. The energy that is stored in the system after charging can be expressed as

$$E_B = \frac{1}{2} C_{\max} V_{start}^2 \tag{2.2}$$

After the variable capacitor has been charged to V_{start}, the electrodes are electrically isolated and the physical separation between the electrode plates is forced to increase due to inertial motion of movable electrode. It is being represented in Fig (7) as the path from point B to point C. This is

the actual step in which mechanical energy is being converted to electrical energy. With an aid of a switch in the energy harvesting circuits S. Roundy et al [2], the electrodes are electrically isolated such that the charges on the electrodes are forced to remain constant from point B to point C. At the same time, the increase in physical separation causes the capacitance of the capacitor to decrease to a minimum value of C_{min}. These two factors lead to an increase in the potential difference across the capacitor.

Specifically, the potential difference increases from V_{start} to V_{max}. When the capacitance has reached C_{min}, the electrical energy stored in the system can be expressed by

$$E_C = \frac{1}{2} C_{\min} V_{\max}^2 \tag{2.3}$$

The last step involved in the energy conversion cycle is the discharging of the charge on the variable capacitor back into the charge reservoir. This is represented by the path from point C to point A in Fig (5), and it concludes one energy conversion cycle. Hence, the amount of energy converted from mechanical to electrical energy in one conversion cycle is

$$E_{conv} = E_c - E_b = \frac{1}{2}(C_{\min} V_{\max}^2 - C_{\max} V_{start}^2) \tag{2.4}$$

By taking into account charge conservation, there is the following relation that we observe the same charges from point B to point C

$$C_{max} V_{start} = C_{min} V_{max}$$

The energy being converted in one energy cycle can thus be rewritten as

$$E_{conv} = E_c - E_b = \frac{1}{2} V_{start}^2 \frac{C_{\max}}{C_{\min}} (C_{\max} - C_{\min}) \tag{2.5}$$

$$E_{conv} = \frac{1}{2} V_{start} V_{\max} (C_{\max} - C_{\min}) \tag{2.6}$$

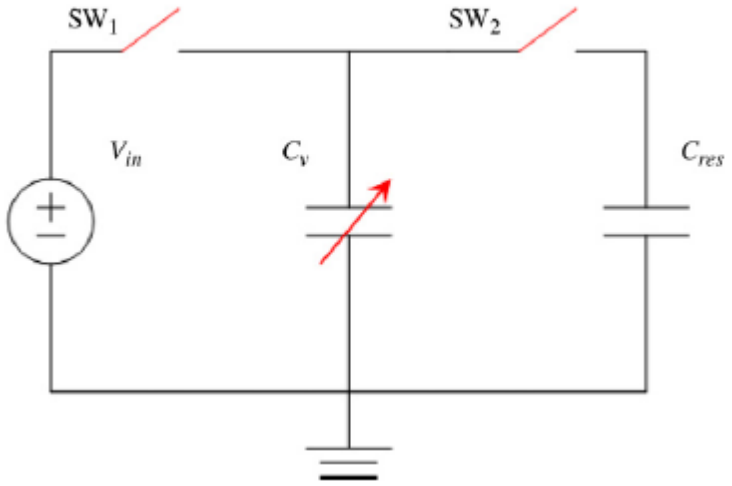

Figure 6: The Schematic circuit of a capacitive converter Geeng-Jen Sheu et al [9].

The charge-constrained cycle starts as the MEMS capacitor C_v (Variable Capacitor) reaches C_{max} with SW1 switch closed and SW2 switch opened, then C_v is discharged from C_{max} to C_{min} with SW1 opened and SW2 closed momentarily to charge the reservoir C_{res} (Reservoir Circuit). Note that, in practice, a circuit using inductors and fly-back diodes is required to minimize the energy loss associated with opening/closing of the switches. The energy conversion per cycle is strongly dependent on C_{max} and C_{min} which are determined by the capacitive structure of the electrostatic comb-drive energy harvester Geeng-Jen Sheu et al [9].

1.9 General Model for Vibration Conversion

A simple forced damped vibration model shown in figure (7) is formulated as general model for the conversion of kinetic energy of a vibrating mass to electrical power based on linear system theory without specifying mechanism by which the conversion is accomplished.

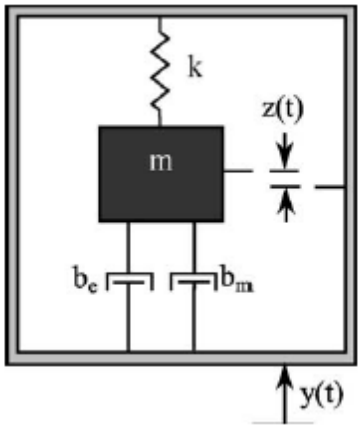

Figure 7: Schematic of generic vibration converter. S. Roundy et al [2]

The model is described by equation (2.7)

$$m\ddot{z} + (b_e + b_m)\dot{z} + kz = -m\ddot{y} \tag{2.7}$$

Where z is the spring deflection, y is the input placement, m is the mass, b_e is the electrically induced damping coefficient, b_m is the mechanical damping coefficient and k is the spring constant.

This model is considered fairly accurate for general studies. Nevertheless, for electrostatic energy scavengers some modification is required. For instance, the relationship between electrical and mechanical system is not necessarily linear any more.

The power converted to electrical system is equal to the power removed from the mechanical system by b_e, the electrically induced damping. The electrically induced force is $b_e \dot{z}$ (power is the product of force and velocity), therefore, power converted is:

$$P = \frac{1}{2} b_e \dot{z}^2 \tag{2.8}$$

Equations (2.7) and (2.8) can be used to derive equation (2.9):

$$P = \frac{m\zeta_e \omega_n \omega^2 \left(\frac{\omega}{\omega_n}\right)^3 Y^2}{\left(2\zeta_T\left(\frac{\omega}{\omega_n}\right)\right)^2 + \left(1-\left(\frac{\omega}{\omega_n}\right)^2\right)^2} \tag{2.9}$$

Where $|P|$ is the magnitude of output power. *Y* the displacement magnitude of input vibrations, ζ_e the electrical damping ratio ($b_e = 2m\zeta_e\omega_n$), ζ_T the combined damping ratio ($\zeta_T = \zeta_e + \zeta_m$), ω the input frequency and ω_n is the natural frequency of spring mass system.

If the spring mass system matches the input frequency, equation (2.9) can be reduced to:

$$P = \frac{m\zeta_e \omega^2 Y^2}{4\zeta_T^2} \tag{2.10}$$

$$P = \frac{m\zeta_e A^2}{4\omega\zeta_T^2} \tag{2.11}$$

Where A is the acceleration of input vibrations.

Note in equation (2.11) that power is inversely proportional to frequency then, if the acceleration magnitude is constant or decreasing with frequency, hence, the design has to meet the lowest fundamental frequency in the input spectrum. Moreover, the output power is proportionally related to mass. Therefore, mass should be chosen to have largest possible value in order to get maximum output power. it is sometimes not practical to apply large mass values due to the design's space limitation which leaves the alternative of using higher frequency vibrations. Previous set of equations assist to determine values of parameters to achieve proper output.

Device Modeling

1.10 Comb-drive Energy Harvester Structure

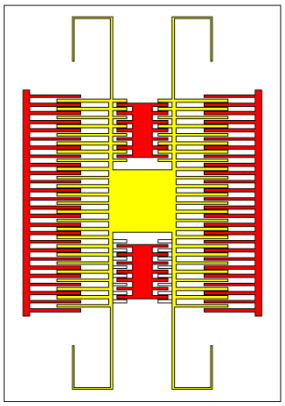

Figure 8: Top view of Energy Harvester

The design consists of three main parts, mechanical springs, comb fingers and vibrating mass. Four mechanical springs support the device and provide needed elasticity for the structure to vibrate. Comb fingers are either fixed -shown in red- or vibrating -shown in yellow- in figure (8). Between fixed and vibrating comb fingers is the capacitive gap in which energy is stored. The vibrating mass provides the excess weight required for the device to vibrate under natural frequency.

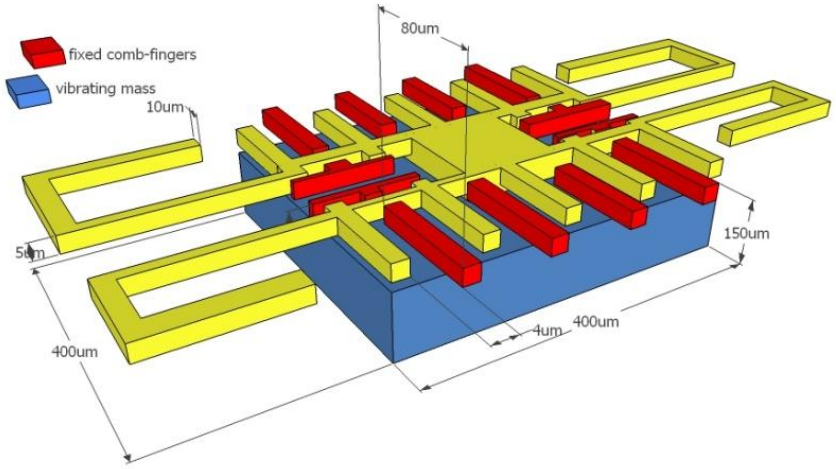

Figure 9: The Comb-Drive Energy Harvester

Fig (9) shows a 3D schematic of the energy harvester in which added mass appears in blue at the bottom of the device. The added mass provides the excess weight required for the device to vibrate under natural frequency.

Table 2: The Energy Harvester Design Parameters

Symbol	Description	values	Unit
L_s	Length of spring	300	μm
t_s	Thickness of spring	5	μm
w_s	Width of spring	10	μm
L_c	Length of comb-finger	80	μm
t_m	Thickness of vibrating mass	150	μm
l_m	Length of vibrating mass	400	μm
w_m	Width of vibrating mass	400	μm
E	Young's modulus of silicon	130	GPa
ρ	Density of silicon	2.33	g/cm^3

Table 2 contains the comb-drive energy harvester structure dimensions and parameters related to silicon, altogether would be used to evaluate the device parameters.

1.11 Evaluation of the Capacitance per Unit Length

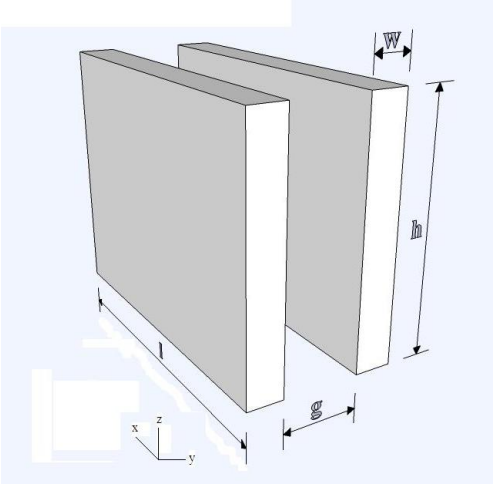

Figure 10: Sketch of typical two plates capacitor

Typical capacitor of a parallel pair of plates has a capacitance value (C) that can be determined in terms of the plate's area (A) and the gap (g) between them. Following equation gives the value of Capacitance:

$$C = \frac{\varepsilon_0 A}{g} = \frac{\varepsilon_0 lh}{g} \tag{4.1}$$

Where ε_0 is vacuum permittivity (8.845×10^{-12} Fm^{-1}), A is the plate's area, g is the gap between plates, l is the plate's length and h is the height of the plates.

Induced driving force and output sensitivity are both proportional to the variation of the capacitance of the comb-drive in the horizontal x axis as stated by Tang W.C. [10]. however, as the movement of comb finger is on the x axis hence the capacitance per unit length is evaluated along the same axis and dented as ($\frac{\partial C}{\partial x}$). By differentiating equation (1):

$$\frac{\partial C}{\partial x} = \frac{\varepsilon_0 h}{g} \tag{4.2}$$

The equation above indicates that capacitance per unit length ($\frac{\partial C}{\partial x}$) is constant and independent of the displacement along the x axis.

Equation (4.2) is used to determine different values of capacitance per unit length ($\frac{\partial C}{\partial x}$) for different values of the capacitor gap (g) and height (h). Result is illustrated on the graph in next page:

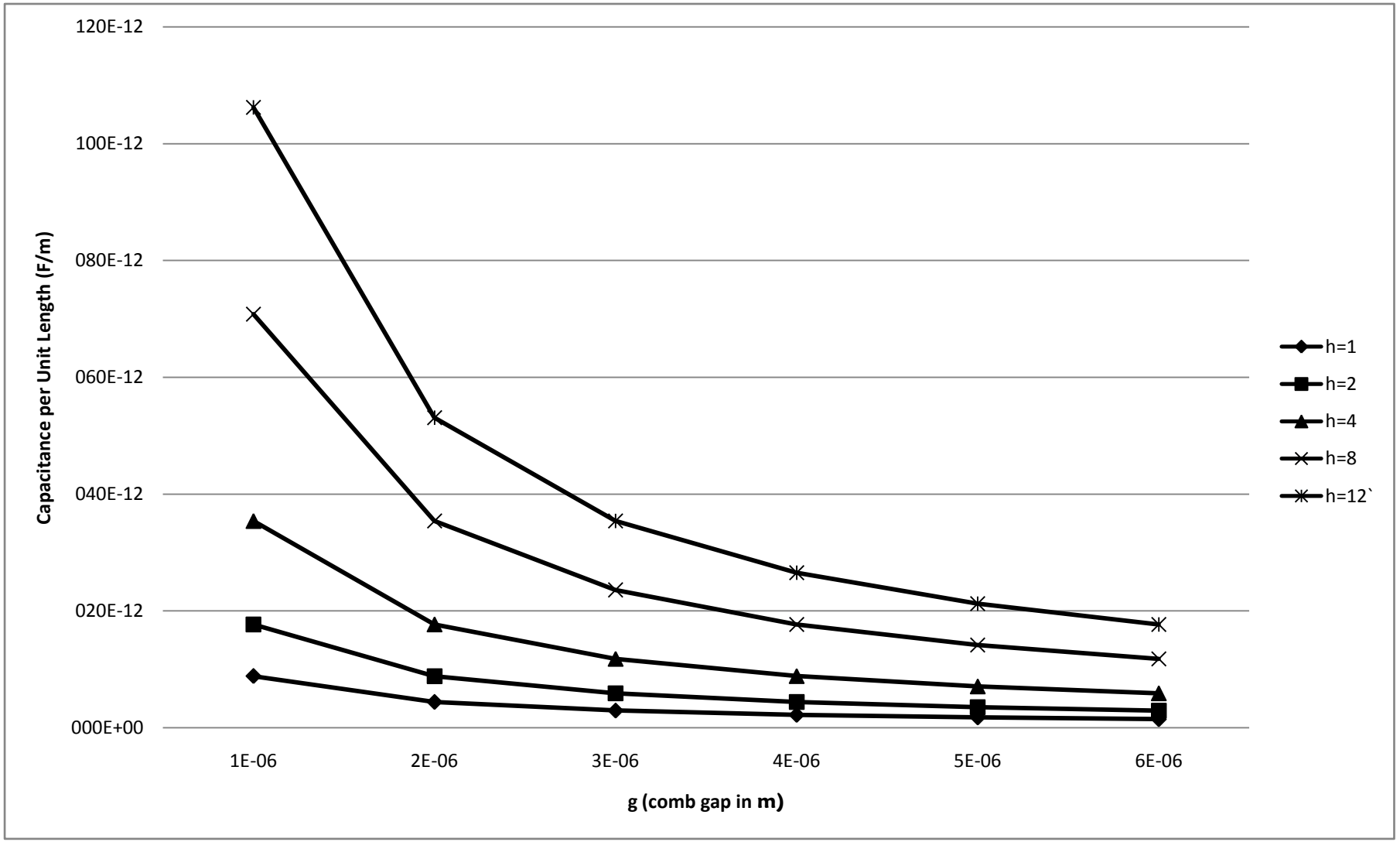

Figure 11 : Capacitance-per-unit-Length ($\frac{\partial C}{\partial x}$) vs comb-drive gap (g)

Obtaining an effective comb-drive energy harvester requires a design with a large value of capacitance per unit length ($\frac{\partial C}{\partial x}$). The graph above shows a dense (large height –h) and small gap fingers would be more desirable to achieve the optimum design.

1.11.1 Evaluation of the Maximum and Minimum Capacitances (C_{max} and C_{min}):

Maximum and minimum capacitors values are very important due to their involvement in the calculation of the comb total output power.

In the in-plane overlap comb drive energy harvester C_{min} is assumed to be zero as the overlapping area between finger and electrodes is also zero during C_{min}. However, during C_{max} the overlapping area increases due to the movement of the finger along the x axis. C_{max} is the total capacitance of two identical capacitors on both sides of the finger connected in parallel.

$$C_{\max} = \frac{2\varepsilon_0 A}{g} = \frac{2\varepsilon_0 lh}{g} \tag{4.3}$$

Where ε_0 is vacuum permittivity (8.845×10^{-12} Fm^{-1}), A is the plate's area, g is the gap between plates, l is the plate's length and h is the height of the plates. In order to determine the effective maximum and minimum capacitors the total number of comb drives on the movable mass should be multiplied by the maximum and minimum capacitors of a single comb finger.

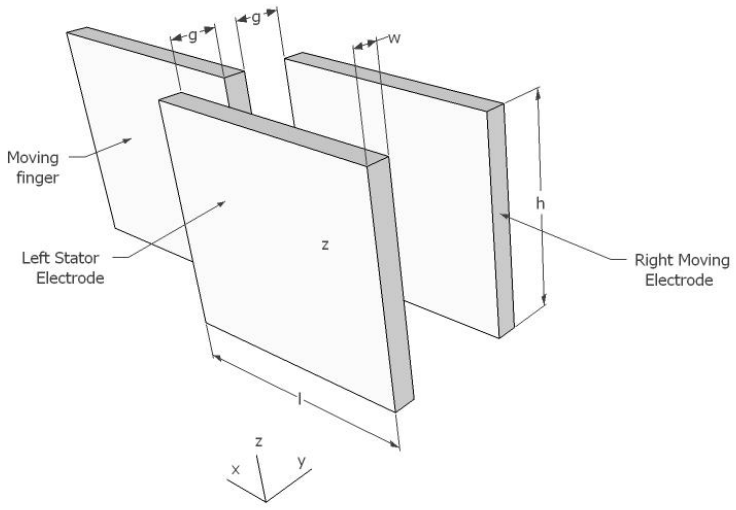

Figure 12 : In-plane-overlap converter in Cmin position (Δx = 0)

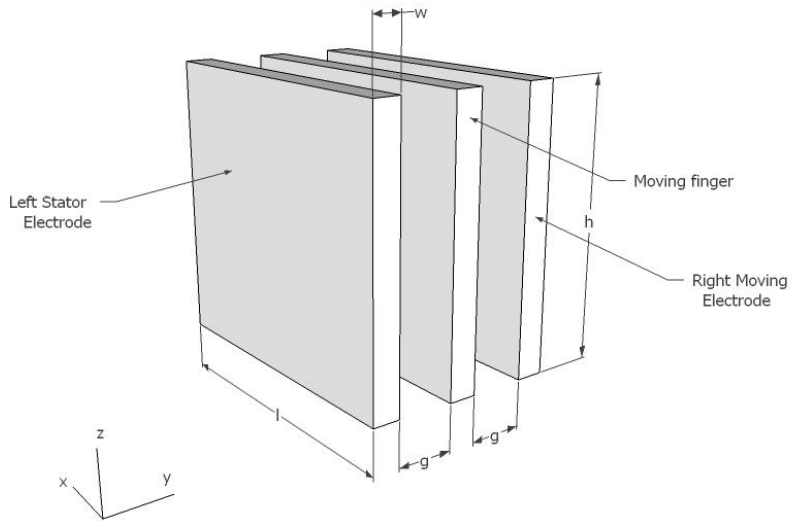

Figure 13 : In-plane-overlap converter in Cmin position ($\Delta x = l$)

1.12 Spring Constant:

1.12.1 Folded-beam suspension design:

This design is chosen due to the fact that it provides free motion for the comb drive along the x-direction and resists unwanted motion along the y-direction. However, the design meets this requirement by having much larger value of the spring constant along the y-axis compared to the spring constant on the x-axis ($k_y >> k_x$).

1.12.2 Spring Constant of Folded-beam Structure:

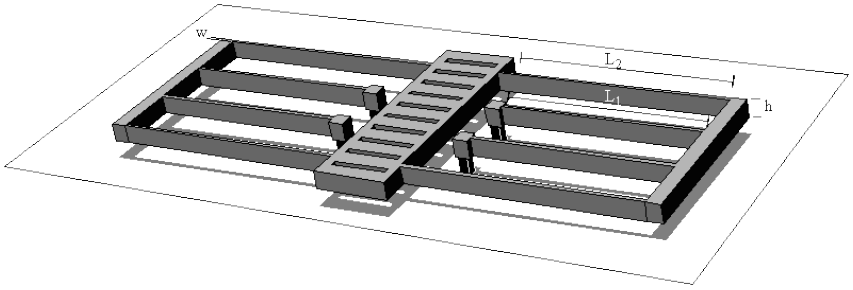

Figure 14: Two Folded-beam structure

the structure presented in Figure13 represents the typical folded beam structure where a mass would suspend on both sides along the x-axis. furthermore, the design is anchored near the centre through 4 points which allows the device to resonate along x-direction while providing resistance to movement along y-direction.

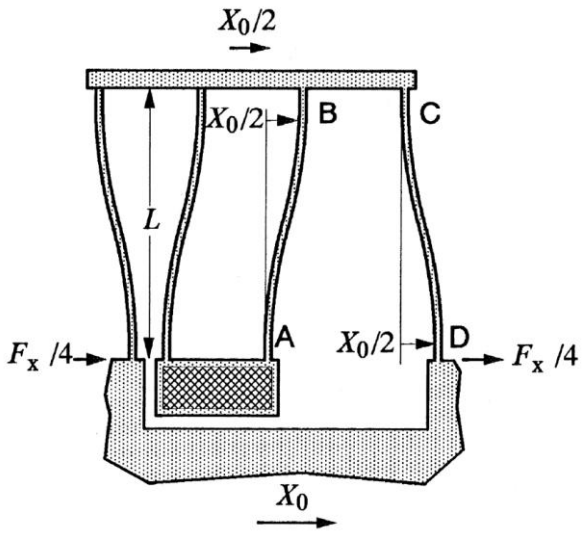

Figure 15: mode shape of a folded beam when force F_x is applied and structure is displaced by X0. Tang [10]

Figure14 was used by Tang [10] to evaluate spring constant to folded-beam structure. The Folded-beam structure consists of four beams each of length L, width w. For more simplification only beam [AB] on the design is used to derive the exact equation of stiffness constant (spring constant) for folded-beam structure.

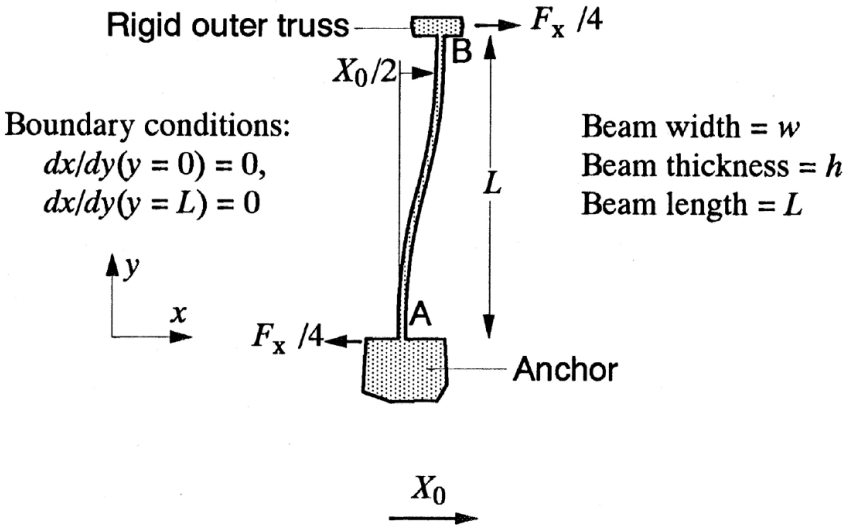

Figure 16:Mode Shape of beam [AB]. Tang [10]

As mentioned on Figure15 the boundary conditions for the deflection equation are:

$$\frac{dx}{dy}(y=0)=0 \tag{4.5}$$

$$\frac{dx}{dy}(y=L)=0 \tag{4.6}$$

then, having the force acting on each folded-beam as $\frac{F_x}{4}$, the deflection equation would be:

$$x(y)=\frac{F_x}{4(12EI_z)}(3Ly^2-2y^3) \qquad \text{for} \qquad 0\le y\le L \tag{4.7}$$

where E is the Young's modulus, I_z is the moment of inertia of the beam cross section with respect to the z axis, L is the beam length.

From Figure15, we can notice that beam [AB] is deflected by $\frac{X_0}{2}$ at point B. Hence, with the boundary condition ($x(L)=\frac{X_0}{2}$), we achieve

$$\frac{X_0}{2}=\frac{F_x}{48EI_z}(3L^3-2L^3)$$

$$\Rightarrow X_0=\frac{F_xL^3}{24EI_z}$$

Then, from the definition of stiffness constant, we get

$$k_x=\frac{F_x}{X_0}=\frac{24EI_z}{L^3} \tag{4.8}$$

Nevertheless, in order to achieve a complete understanding of the spring constant, moment of inertia (I_z) should be expressed in terms of the beam's dimensions. In this particular case, moment of inertia for an ideal beam with rectangular cross section with width w and thickness h can be used to find the value of I_z, hence I_z is given by

$$I_z = \frac{hw^3}{12} \tag{4.9}$$

As stated earlier, the folded-beam structure provides resistance to the motion on the y-direction only if condition ($k_y >> k_x$) is satisfied. However, the constant (k_y) along y-direction needs firstly to be evaluated. Calculation of k_y is not the same as calculation of k_x. As the device would be in tension or compression mode, then axial stiffness equation would suit the case. k_y is given by:

$$k_y = \frac{AE}{L} \tag{4.10}$$

where A is the cross section area of the beam, E is the Young's modulus and L is the length of the beam. To satisfy the condition mentioned above, a constant ratio should be maintained between k_x and k_y. For the case provided by Tang the ratio is 8. hence:

$$\frac{8k_y}{k_x} = \frac{8AE/L}{24EI_z/L^3} = \frac{AL^2}{3I_z}$$

applying equation (4.9) and ($A = wh$):

$$\frac{8k_y}{k_x} = \frac{4L^2}{w^2} \tag{4.11}$$

From equation (7) we can see for a folded-beam structure with L=200μm and w=2μm, k_y is 40,000 times larger than k_x. which perfectly satisfies the condition ($k_y >> k_x$).

Methodology

1.13 Project Flow Chart

The diagram shown below briefly explains the stages through which the project will be accomplished. The methodology is divided into two phases, first phase to be accomplished during FYP1 and the second during FYP2. In the first phase research about the background of the project is done and information is gathered to have a good clue about the background of the project and theory involved.

In the second phase, mathematical model of the device is to be acquired and established accurately and then analyzed critically using MATLAB. Then once the mathematical model is prepared and ready to be keyed into the MEMS simulation software (CoventorWare) in order to build the Model. The next stage is to analyze and discuss the results acquired by the two softwares to achieve the conclusion and recommendations.

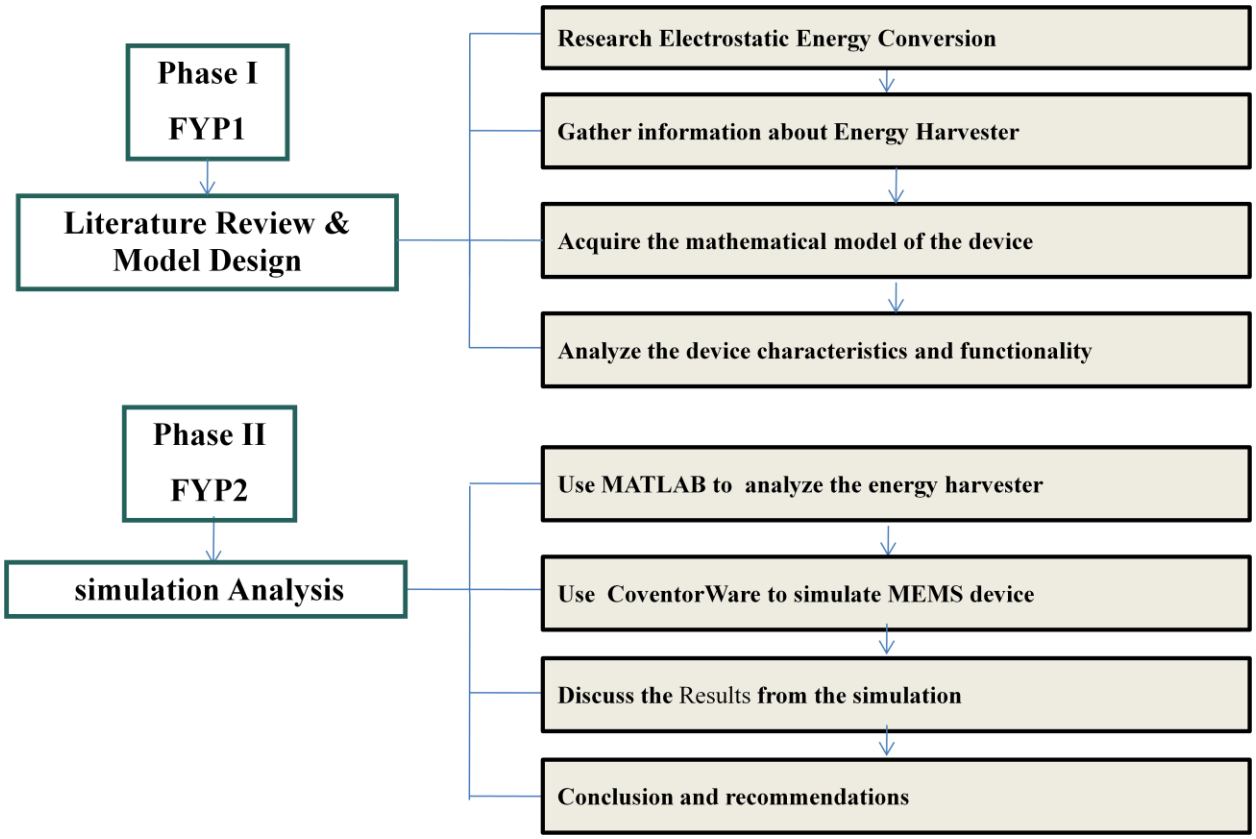

Figure 17 : Project Flow Chart

1.14 Gantt Chart FYP1

Table 3: Gantt Chart

No	Detail/Week	1	2	3	4	5	6	7	8	9	10	11	12	13	14
1	Topic Selection / Proposal							Mid Semester Break							
2	Preliminary Research Work														
3	Submission of Proposal Defense Report						★								
4	Proposal Defense (Oral Presentation)									★					
5	Project Work Continues														
6	Submission of Interim Draft Report													★	
7	Submission of Interim Report														★

★ **Milestone**

1.15 Gantt Chart FYP2

NNO	Detail/Week ail/Week	1	2	3	4	5	6	7		8	9	10	11	12	13	14
1	Project work continue								Mid Sem Break							
2	Submission of progress report 1															
3	Project work continue															
4	Submission of progress report 2									★						
5	Seminar															
5	Project work continue															
6	Oral Presentation															
7	Poster Exhibition												★			
8	Submission of Dissertation (draft)													★		
9	Submission of Dissertation (Soft Bound)														★	

★ Milestone

Results and Discussion

1.16 Evaluation of Equation of Motion

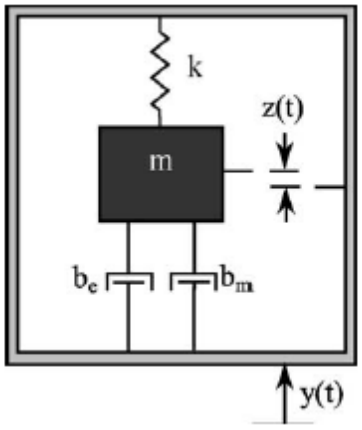

Figure 18: Schematic of generic vibration converter. S. Roundy et al [2]

the model is described by

$$m\ddot{x} + c\dot{x} + kx = -m\ddot{y}$$

by using the following equations:

$$\omega^2 = \frac{k}{m}, \qquad \zeta = \frac{c}{2m\omega}$$

A proper representation is

$$\ddot{x} + 2\zeta c\dot{x} + \omega^2 x = F_0 \cos wt$$

The complete solution of the equation is the sum of the natural and forced response

$$x(t) = x_h(t) + x_p(t)$$

The natural response is given by

$$x_h(t) = X_0 e^{-\zeta w_n t} \cos(\omega_d t - \phi_0)$$

Where $\omega_d = \sqrt{1-\zeta^2}\,\omega_n$

Forced response is assumed to be in the form

$$x_p(t) = X\cos(\omega t - \phi)$$

Then complete solution is given by

$$x(t) = X_0 e^{-\zeta\omega_n t}\cos(\omega_d t - \phi_0) + X\cos(\omega t - \phi)$$

Where

$$\omega_n = \sqrt{\frac{k}{m}}$$

$$\zeta = \frac{c}{2m\omega}$$

$$r = \frac{\omega}{\omega_n}$$

$$\delta_{st} = \frac{F_0}{k}$$

$$\frac{X}{\delta_{st}} = \frac{1}{\sqrt{\left(1-r^2\right)^2 + \left(2\zeta r\right)^2}}$$

$$\phi = \tan^{-1}\left(\frac{2\zeta r}{1-r^2}\right)$$

$$X_0 = \left[\left(x_0 - X\cos\phi\right)^2 + \frac{1}{\omega_d^2}\left(\zeta\omega_n x_0 + \dot{x}_0 - \zeta\omega_n X\cos\phi - \omega X\sin\phi\right)^2\right]^{\frac{1}{2}}$$

$$\tan\phi_0 = \frac{\zeta\omega_n x_0 + \dot{x}_0 - \zeta\omega_n X\cos\phi - \omega X\sin\phi}{\omega_d\left(x_0 - X\cos\phi\right)}$$

m	Total mass	ζ	Damping ratio
x	displacement	c	Damping constant
k	Spring constant	r	Frequency ratio
ω	Undamped natural frequency	δ_{st}	Deflection under the static force F_0

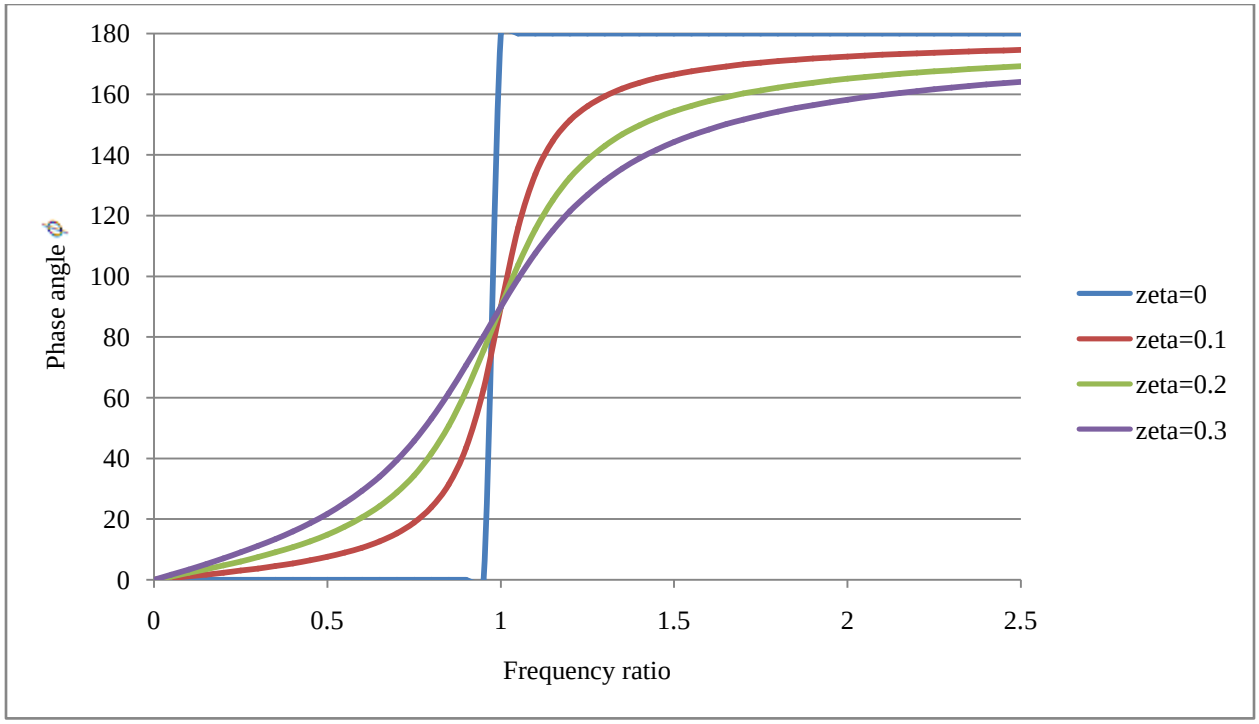

Figure 19: variation of phase angle vs frequency ratio r

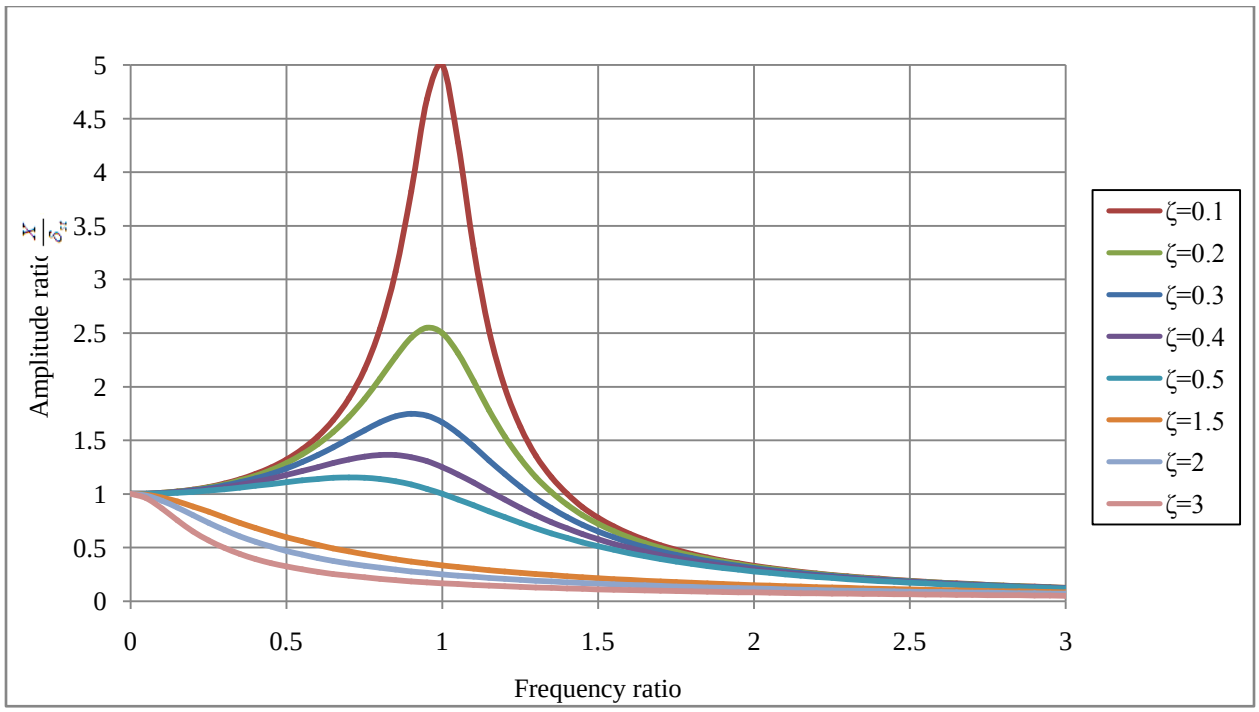

Figure 20 : Variation of amplitude vs frequency ratio r

1.17 Evaluation of Spring Constant

As shown in section 3.1, the device structure is supported by four springs, each with 1000μm, 4μm,50μm length, width and thickness respectively and denoted as (l_s,w_s and t_s).

To find total springs constant, a singles spring constant is calculated first then as the four springs are connected in parallel then the calculated value is multiplied by 4.

Table 4: Values to calculate spring constant

Symbol	Description	values	Unit
L_s	Length of spring	400	μm
t_s	Thickness of spring	50	μm
w_s	Width of spring	10	μm
E	Young's modulus of silicon	130	GPa
ρ	Density of silicon	2.33	g/cm^3

$$I = \frac{t * w_s^3}{12} = \frac{5*10^{-6} * (10*10^{-6})^3}{12} = 4.167*10^{-22}\, kg.m^2$$

$$k_{\sin gle} = \frac{2*12*E*I}{l_s^3} = \frac{6*130*10^9 *1.429*10^{-22}}{(500*10^{-6})^3} = 16.52.N/m$$

$$k_{total} = 4 * k_{\sin gle} = 4*16.52 = 65.04N/m$$

1.18 Evaluation of Natural Frequency (ω_n)

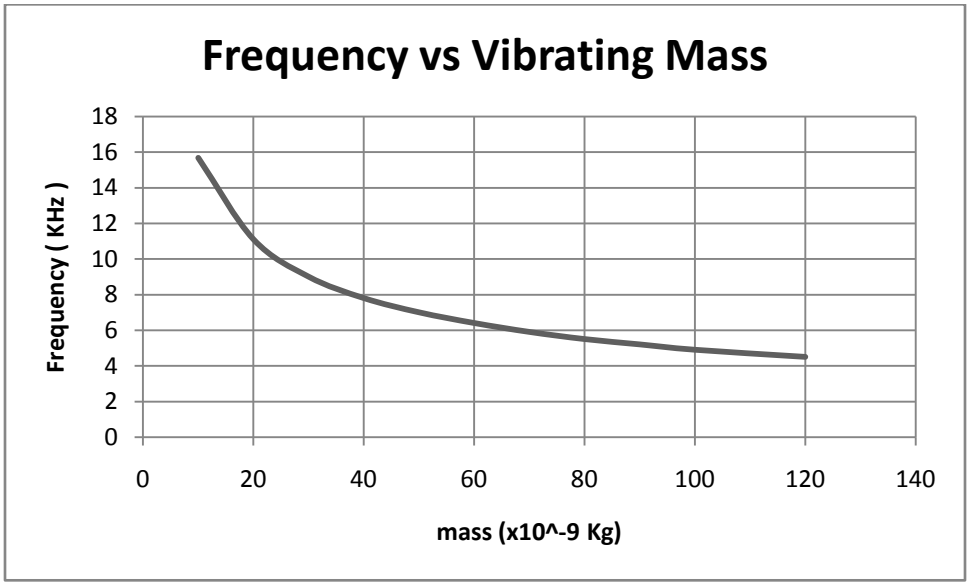

Figure 21 : Frequency vs Vibrating Mass

The graph in Fig 21 illustrates the relationship between vibrating mass and resulting output frequency. It is stating that with increasing the mass value less output frequency is obtained.

According to Fabrim.E [15] the equivalent effective mass of device is found by:

$$M_e = \frac{13m_v}{35} + m_B$$

Where M_e is effective equivalent mass, m_v is the total spring mass and m_B is the excess mass (vibrating mass).

Table 5: Values for natural frequency calculation

Symbol	Description	values	Unit
L_s	Length of spring	500	μm
t_s	Thickness of spring	5	μm
w_s	Width of spring	10	μm
L_c	Length of comb-finger	80	μm
t_m	Thickness of vibrating mass	150	μm
l_m	Length of vibrating mass	400	μm
w_m	Width of vibrating mass	400	μm
ρ	Density of silicon	2.33	g/cm^3

Total spring mass for this structure is four times single structure mass:

$$m_v = 4 * \rho * l_s * w_s * t_s = 4 * 2.33 * 10^3 * 500 * 10^{-6} * 10 * 10^{-6} * 5 * 10^{-6} = 1.09212 * 10^{-8} kg$$

Vibrating mass is:

$$m_B = \rho * l_m * w_m * t_m = 2.33 * 10^3 * 400 * 10^{-6} * 400 * 10^{-6} * 150 * 10^{-6} = 5.59 * 10^{-8} kg$$

Effective mass:

$$M_e = m_v + m_B = 6.68412 * 10^{-8} kg$$

Natural frequency:

$$f_n = \frac{1}{2\pi}\sqrt{\frac{k_{total}}{M_e}} = \frac{1}{2\pi}\sqrt{\frac{65.04}{6.68412 * 10^{-6}}} = 5003.396 Hz = 5 KHz$$

1.19 Evaluation of Output Power

1.19.1 Mechanical Damping

N	Number of capacitive gaps	124	
μ	Dynamic viscosity of air	$1.85*10^{-5}$	kg.s
w	Width of comb finger	10	μm
d	Capacitive gap distance	4	μm
M	Equivalent mass	$4.9922*10^{-6}$	kg
ω_n	Angular frequency	314159	rad/s

Table 6: : Table for Mechanical Damping Calculation

Mechanical damping is represented by coutte flow (when fluid flows in the space between two parallel plates where one is moving relative to the other).

$$\zeta_m = \frac{\mu N l w}{d} x \frac{1}{2M\omega_n} = \frac{1.85*10^{-5}*124*4*10^{-12}}{2*4*10^{-12}*4.9922*10^{-6}*666} = 0.00104267$$

1.19.2 Electrical Damping

Table 7: : Table for Electrical Damping Calculation

N	Number of capacitive gaps	124	
ε_0	Dynamic viscosity of air	$8.85*10^{-12}$	F/m
t	thickness of comb finger	5	μm
d	Capacitive gap distance	4	μm
M	Equivalent mass	$6.68412*10^{-8}$	kg
ω_n	Angular frequency	314159	rad/s

The electrical damping is represented by force acting on capacitors:

$$C = \frac{\varepsilon t l}{d}$$

$$F_e = -\frac{dW_e}{dx} = \frac{1}{2}V^2\frac{dC}{dx} = N\frac{\varepsilon t}{2d}V^2$$

$$\zeta_e = \frac{\varepsilon_0 V_{high} Nw}{2d} x \frac{1}{2M\omega_n} = \frac{8.85*10^{-12}*30*100*50*10^{-6}}{4*4*10^{-6}*4.9922*10^{-6}*666} = 0.07485215$$

1.19.3 Total Damping

$$\zeta_T = \zeta_e + \zeta_m = 0.0758948$$

1.19.4 Displacement

Table 8 : : Table for Displacement Calculation

Y_0	Input amlitude	10	μm
k	Spring constant	65.04	N/m
ω	Input angular frequency	ω_n	
ω_n	Angular frequency	314159	rad/s
ω_c	Frequency ratio $\frac{\omega}{\omega_n}$	1	ω_c
M	Equivalent mass	$6.68412*10^{-8}$	kg

$$X = \frac{Y_0}{k*\sqrt{\left(1-\omega_c{}^2\right)^2 + \left(2\zeta\omega_c\right)^2}} = \frac{10*10^{-10}}{65.04*0.0206*0.00179188} = 0.832\text{um}$$

- Output Power:

$$P = \frac{M\zeta_e\omega_n\omega^2\left(\frac{\omega}{\omega_n}\right)^3 Y_0{}^2}{\left(2\zeta_T\left(\frac{\omega}{\omega_n}\right)\right)^2 + \left(1-\left(\frac{\omega}{\omega_n}\right)^2\right)^2}$$

In case of having input frequency the same as natural frequency yields:

$$P = \frac{M\zeta_e\omega^2 Y_0{}^2}{4\zeta_T^2} = \frac{6.68412*10^{-8}*0.0007485*666^2*(10*10^{-6})^2}{4*(0.00179188)^2} = 0.2949\mu\text{watts}$$

1.19.5 Maximum Capacitance

Table 9: : Table for Maximum Capacitance Calculation

N	Number of capacitive gaps	124	
ε_0	Dynamic viscosity of air	$8.85*10^{-12}$	F/m
t	thickness of comb finger	5	μm
d	Capacitive gap distance	4	μm
M	Equivalent mass	$6.68412*10^{-8}$	kg
ω_n	Angular frequency	314159	rad/s

$$C_{\max} = \frac{2N\varepsilon_0 A}{d} = \frac{2N\varepsilon_0 lt}{d} = \frac{2*8.85*10^{-6}*300*50*10^{-12}}{4*10^{-6}} = 6.6405x10^{12}\,F$$

1.19.6 Energy per Cycle

Starting voltage is in the range : $0 \le V_{start} \le 5$

Maximum value is 30V.

$$E = \frac{1}{2}V_{start}V_{\max}C_{\max} = \frac{1}{2}*2.5*30*6.6405*10^{-12} = 2.49nJ$$

1.19.7 Simulation Results

The simulation output matches the calculation giving an output frequency of 5 KHz with a slight deviation which is due to rounding in calculations.

The energy harvester device model is Simulated by CoventorWare based on 0.35 µm CMOS standard process. CMOS process has different layers, 3 layers are of aluminum -metal- separated by insulation layers which are of silicon dioxide. The 5 layers comprises a thickness of 5µm. Figure (22) illustrates shows all different layers which make the energy harvester.

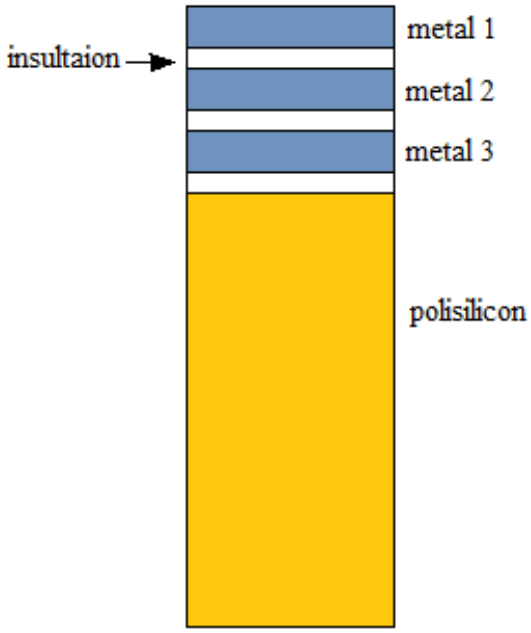

Figure 22: Schematic cross section of the device

The CoventorWare produces the complete model of the energy harvester after going through few steps. First, Designer produces the 3-D model as shown in Fig (23).

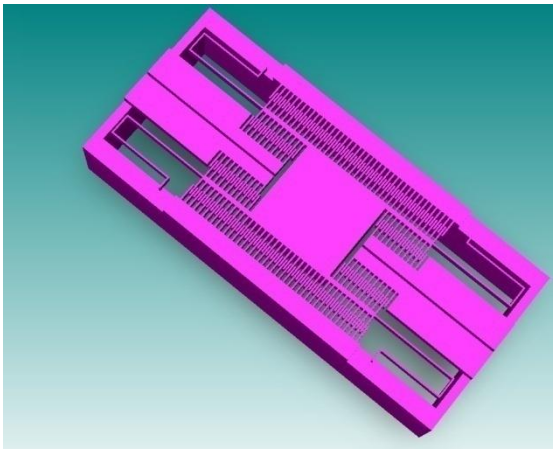

Figure 23: 3-D Layout of Energy Harvester

Figure (24) shows the DRIE etching of the back-side of the silicon wafer.

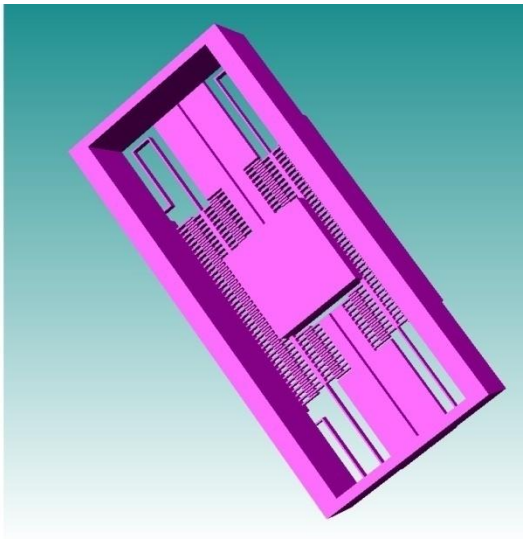

Figure 24: Etching from back side

The following step is meshing. The 3-D model of the energy harvester has to be meshed in order to divide the structure into small finite elements to be applied to the finite element method (FEM) in CoventorWare. Then tetrahedral mesh type is used to obtain simulation results.

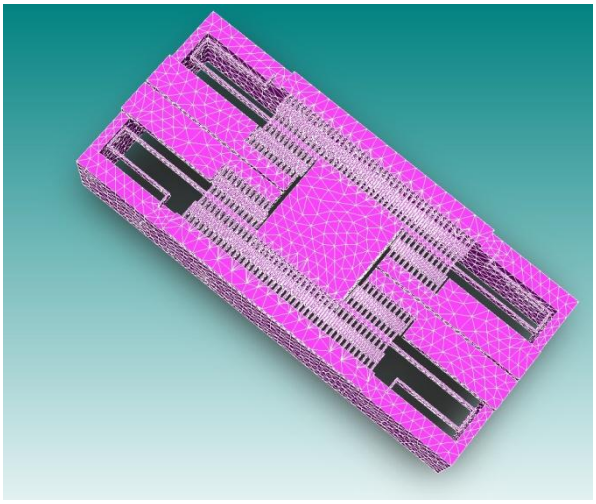

Figure 25: 3-D meshed model

.

Fig (261) shows the CoventorWare simulation results where FEM is used to obtain the model and natural frequency is shown as 5 KHz which corresponds to the theory discussed in modeling.

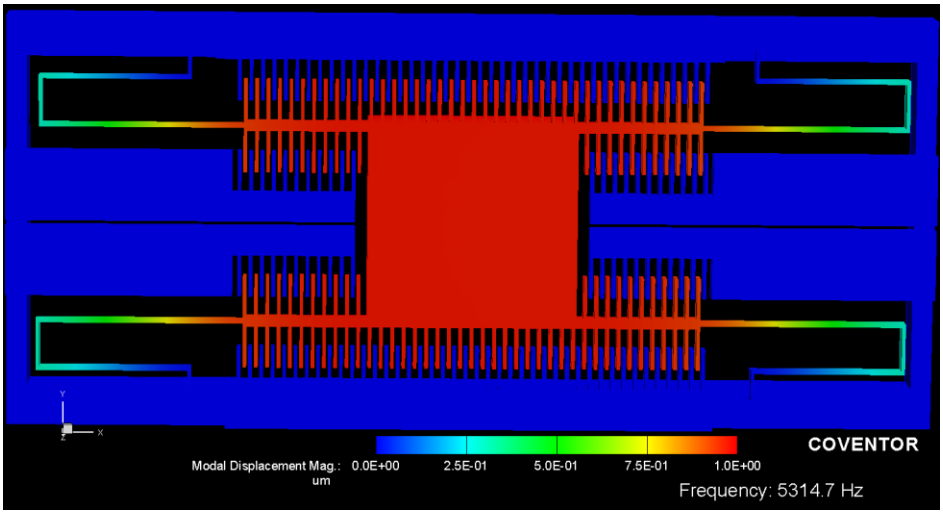

Figure 26: 2-D FEM simulation result

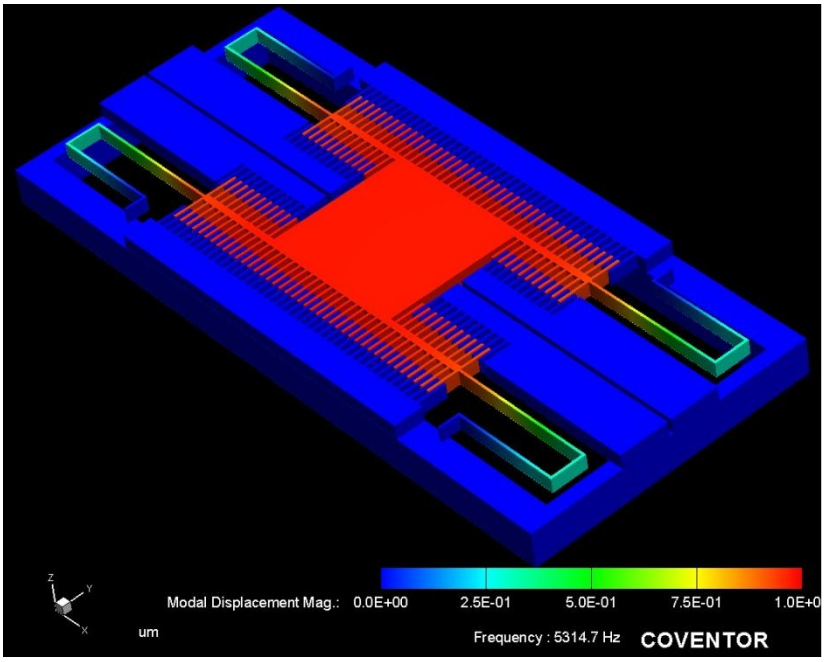

Figure 27: 3-D FEM simulation result

Conclusion

An electrostatic energy harvester to be used for powering up wireless sensor nodes is designed and simulated using CoventorWare software. The energy harvester works in the charge-constraint cycle which is more compatible with CMOS technology rather than voltage-constrained cycle. The device is modelled by a simple forced damped vibration model that represents the device and explains more about vibration mode. From the damped model equation displacement of the energy harvester was found to be 1 µm when device vibrates with 5 KHz as natural frequency. An extra mass of 400µmx400µmx150µm is added at the bottom of the energy harvester to achieve the required resonant frequency. The energy harvester utilizes 124 comb fingers distributed all over the structure to harvest and scavenge vibration into electric energy.

CMOS standard technology process which comprises metal and dielectric layers. DRIE is also applied to etch back-side of the energy harvester as well as front side in order to release the structure and allow for free movement for the vibrating mass.

CoventorWare software is used to create the energy harvester. CoventorWare created the 3-D model first then meshed the model to acquire precise results when using finite element method (FEM). FEM simulation has resulted in a resonant frequency of 5KHz. The simulation result concludes that theory matches properly with simulation.

References

[1] Scott Meninger, Jose Oscar Mur-Miranda, Rajeevan Amirtharajah, Anantha P. Chandrakasan, and Jeffrey H. Lang, Fellow, IEEE. 2001. Vibration-to-Electric Energy Conversion. 64-76.

[2] S. Roundy, P.K. W';right, J. Rabaey, A study of low level vibrations as a power source for wireless sensor nodes, Comput. Commun. 26 (2003) 1131–1144.

[3] Ahmed Nounou. Hani F. Ragaie A lateral Comb-Drive Structure or Energy Scavenging. (2004) 553 – 556.

[4] Chengkuo Leea,b,_, Ye Mei Lima, Bin Yangb, Rama Krishna Kotlankab, Chun-Huat Henga, Johnny Han Heb, Min Tangb, Jin Xieb,sna.2009.02.024. 208 – 216. Theoretical comparison of the energy harvesting capability among various electrostatic mechanisms from structure aspect.

[5] Michael M. Tilleman, *"Analysis of electrostatic comb-driven actuators in linear and nonlinear regions"* 2004.

[6] Glynne-Jones P, Tudor M J, Beeby S P and White N M, *"An electromagnetic, vibration-powered generator for intelligent sensor systems "*2004.Sensors Actuators A 110 344–9. 2004.

[7] El-Hami M, Glynne-Jones P, James E, Beeby S P, White N M, Brown A D, Ross J N and Hill M, *"Design and fabrication of a new vibration-based electromechanical power generator"* 2001.Sensors Actuators A 92 335–42. 2001.

[8] S P Beeby, M J Tudor and N M White, "*Energy harvesting vibration sources for micro systems applications"* Meas. Sci. Technol. 17 (2006) R175–R195.

[9] Geeng-Jen Sheu, Shih-Ming Yang and Tehsi Leeb, "Development of a low frequency electrostatic comb-drive energy harvester compatible to SoC design by CMOS process". Sensors and Actuators A 167 (2011) 70–76.

[10] Tang W.C. PH.D thesis 1990 "Electrostatic Comb Drive for Resonant Sensor and Actuator Applications

[11] Chiu Yi et al. 2006 "MEMS design and fabrication of an electrostatic vibration-to-electricity energy converter".

[12] W. C. Tang, “Electrostatic comb drive for resonant sensor and actuator applications,” Ph.D. dissertation, Department of Electrical Engineering and Computer Sciences, University of California, Berkeley, USA, 1992.

[13] Singireso S.RAO. Mechanical Vibrations. Fifth edition. 2011.

[14] Shashank Priya, Daniel J.Inman..Energy Harvesting Technologies. 2009.

[15] Fabrim.E et al. Natural Vibration Frequency of classis MEMS Structures.

Appendices

1.20 Appendix I

Moment of inertia for rectangular cross section area across z-axis

$$I_z = \int x^2 dA = \int_{-\frac{w}{2}}^{\frac{w}{2}} \int_{-\frac{h}{2}}^{\frac{h}{2}} x^2 dz dx = 2h \int_0^{\frac{h}{2}} x^2 dx = 2h \left[\frac{x^3}{3} \right]_0^{\frac{w}{2}} = \frac{hw^3}{12}$$

$$I_z = \frac{hw^3}{12}$$

1.21 Appendix II

Natural Frequency Matlab code

```
%spring constant
spring_l=400*10^-6;                    %spring length
spring_w=10*10^-6;                      %spring width
t=5*10^-6;                             %structure height
E=130*10^9;                             %young's modulus
I=(t*(spring_w)^3)/12                   %moment of inertia
k_single=(2*12*E*I)/((spring_l)^3)      %single beam
stiffness
k_total=4*k_single                      %total stiffness

%spring mass
dens=2.33*10^3;                         %density of silicon in
kgm^-3
m_spring=spring_l*spring_w*t*dens       %single spring mass in
kg
m_spring_total=4*m_spring               %total spring mass in
kg

%vibrating fingers mass
finger_l=100*10^-6;
finger_w=7*10^-6;
finger_t=54*10^-6;
N=124;
m_finger_total=N*dens*finger_l*finger_w*finger_t

%vibrating mass
vibrating_mass_l=400*10^-6;
vibrating_mass_w=400*10^-6;
vibrating_mass_t=150*10^-6;

m_vibrating_mass=dens*vibrating_mass_l*vibrating_mass_w*vib
rating_mass_t

%total vibrating mass
m_vibrating_total=m_vibrating_mass+m_finger_total


%natural frequency
f=sqrt(k_total/m_vibrating_total)/(2*pi)
```